NANO LETTERS

pubs.acs.org/NanoLett Letter

Ferroelectric Switching of Pure Spin Polarization in Two-Dimensional Electron Gas

Er-Wei Du,[#] Shi-Jing Gong,*,[#] Xiaodong Tang, Junhao Chu, Andrew M. Rappe,* and Cheng Gong*

Cite This: https://dx.doi.org/10.1021/acs.nanolett.0c02584 Read Online

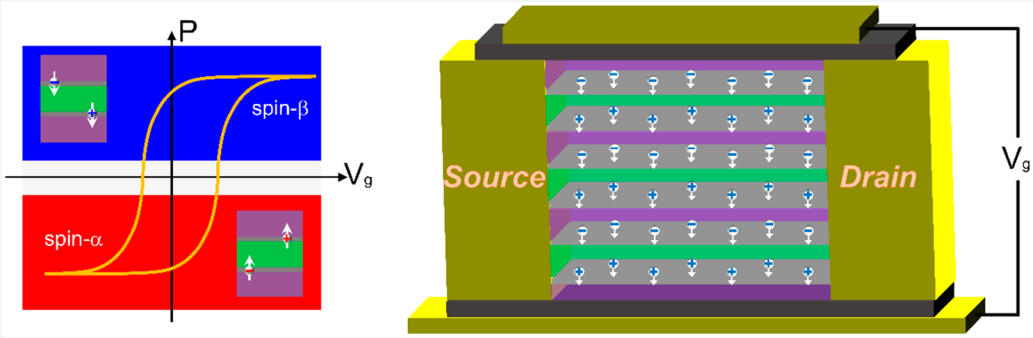

ABSTRACT: Two-dimensional electron gas (2DEG) created at compound interfaces can exhibit a broad range of exotic physical phenomena, including quantum Hall phase, emergent ferromagnetism, and superconductivity. Although electron spin plays key roles in these phenomena, the fundamental understanding and application prospects of such emergent interfacial states have been largely impeded by the lack of purely spin-polarized 2DEG. In this work, by first-principles calculations of the multiferroic superlattice GeTe/MnTe, we find the ferroelectric polarization of GeTe is concurrent with the half-metallic 2DEG at interfaces. Remarkably, the pure spin polarization of the 2DEG can be created and annihilated by polarizing and depolarizing the ferroelectrics and can be switched (between pure spin-up and pure spin-down) by flipping the ferroelectric polarization. Given the electric-field amplification effect of ferroelectric electronics, we envision multiferroic superlattices could open up new opportunities for low-power, high-efficiency spintronic devices such as spin field-effect transistors.

KEYWORDS: *Two-dimensional electron gas, multiferroics, half-metal, ferroelectric control, spin field-effect transistor*

Controlling the spin degree of freedom by pure electrical means holds great significance in energy-efficient spintronic devices. However, the external electrical field is typically several orders of magnitude weaker than the materials' crystal field and electrostatic doping usually can only modulate the carrier concentration at the level of 10^{12}−10^{13} /cm^2 (equivalent of 0.001−0.01 electrons per atom); thus, both schemes are unable to deliver efficient electrical control of magnetism. In contrast, leveraging the inherent magnetoelectric coupling in multiferroic materials[1−6] provides an outstanding possibility, due to the intrinsic coupling between electrical order and magnetic order. Among many multiferroics,[7−26] artificial multiferroic heterostructures possess much more freedom in material choices and combinations, and meanwhile, owing to the mechanical deformation related to the ferroelectric polarization, the magnetism can be prominently controlled.[16−25] However, due to the large band gaps of the insulating multiferroics, most of them are impractical for spintronic transport, and multiferroic heterostructures consisting of semiconductors are highly desirable.

As a prototype of ferroelectric Rashba semiconductors,[27−29] GeTe crystallizes in a trigonal ferroelectric phase (space group *R*3*m*) below 720 K.[28−30] Bulk MnTe, a semiconducting A-type antiferromagnet with the Néel temperature $T_N \sim 310$ K,[31−34] crystallizes in the hexagonal NiAs structure, and thus is likely to be able to be integrated with GeTe to form multiferroics. Indeed, $Ge_{1-x}Mn_xTe$ compound has been widely investigated both experimentally and theoretically.[35−40] It was found that the doping of GeTe with Mn atoms maintains the rhombohedral lattice distortion and ferroelectricity in $Ge_{1-x}Mn_xTe$ ($x < 0.3$),[38] in which Mn spins ferromagnetically couple to each other via free-carrier-mediated RKKY (Ruderman−Kittel−Kasuya−Yosida) exchange interactions with the Curie temperature up to ∼200 K.[41,42] However, as evident, the deleterious effects associated with the doping scheme (e.g.,

Received: June 22, 2020
Revised: August 12, 2020
Published: August 12, 2020

enhanced impurity scattering and reduced Curie temperature) remain in $Ge_{1-x}Mn_xTe$.

The GeTe/MnTe heterostructures, as high-quality crystals, potentially circumvent the deleterious effects in doping compounds and may possess properties that are unexpected in constituent bulk materials and doping compound $Ge_{1-x}Mn_xTe$. In this article, a GeTe/MnTe multiferroic superlattice is constructed, and the resultant multiferroicity is studied. Surprisingly, we find that the ferroelectric polarization of GeTe can produce half-metallic two-dimensional electron and hole gases (2DEG and 2DHG) at the alternating interfaces of the superlattice. Interestingly, these 2DEG and 2DHG have the same spin orientation. When the ferroelectric polarization of GeTe is reversed, the spin direction is reversed. In short, the pure spin polarization can be created and annihilated by polarizing and depolarizing the ferroelectric and can be switched (between pure spin-up and pure spin-down) by flipping the ferroelectric polarization.

We design a superlattice consisting of a ferroelectric semiconductor and an A-type antiferromagnetic semiconductor (i.e., intralayer ferromagnetism and interlayer antiferromagnetism), which is illustrated in Figure 1a. The ferroelectric

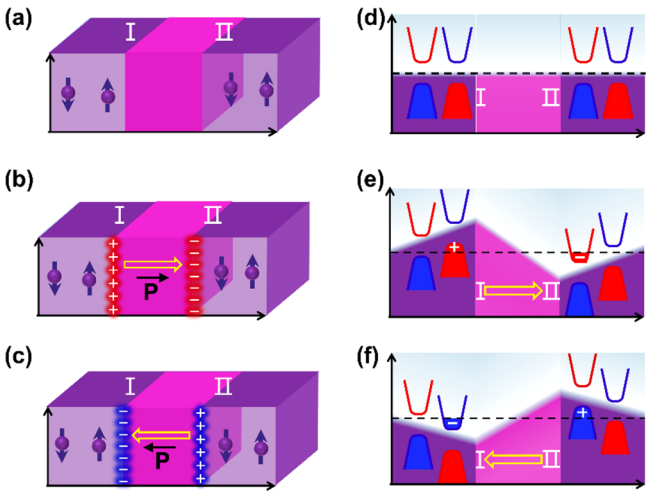

Figure 1. (a−c) The schematic structures of the ferroelectric/A-type antiferromagnet superlattices and the change of the interfacial states induced by the ferroelectric polarization reversal. The schematic electronic structures in parts d−f correspond to the structures in parts a−c, respectively. The ferroelectric polarization $\vec{p}$ is zero in parts a and d. I and II indicate the two interfaces. The ferroelectric polarizations indicated by the arrows are pointing to the right in part b and to the left in part c, respectively. "+" and "−" in parts b and c indicate holes and electrons accumulated at the interfaces. Red and blue colors in parts b−f indicate the spin-α and -β bands/carriers, respectively.

layer is sandwiched between the neighboring A-type antiferromagnetic layers, forming the two interfaces I and II. When the ferroelectric polarization is zero (as illustrated in Figure 1a), the two adjacent antiferromagnets have the same electrostatic potential and the energy levels of the two adjacent interfaces are identical (Figure 1d). However, when the ferroelectric is polarized (Figure 1b,c), the electrostatic potential gradient will be induced in the two adjacent antiferromagnets (Figure 1e,f) with asymmetry between the interface I and II. That is, there are equal amounts of electrons and holes of the same spin orientation on the two interfaces, respectively. The spin polarization of these 2DEG and 2DHG can be reversed by flipping the ferroelectric polarization.

A practical material platform for the above concept is the GeTe/MnTe superlattice. Bulk GeTe acquires a spontaneous polarization as large as ∼60 $\mu C/cm^2$ along the 3-fold axis of the rhombohedral cell.[28,29] Its primitive unit cell is shown in Figure 2a, in which Ge and Te ions are displaced from the

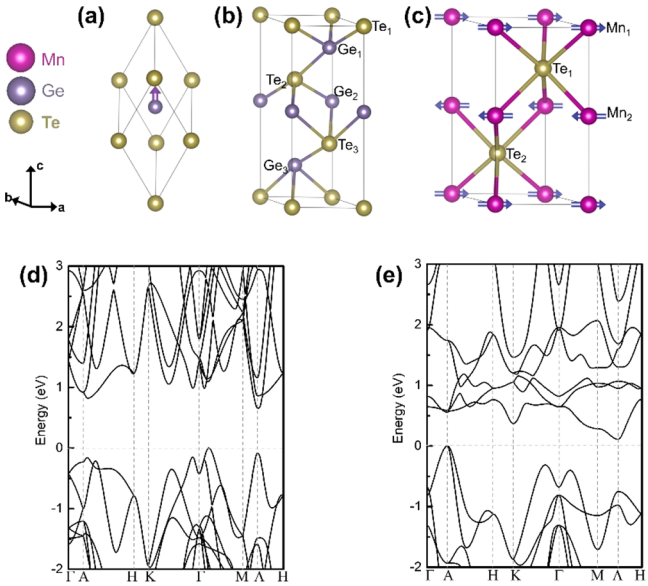

Figure 2. Atomic structures of GeTe and MnTe and their band structures. (a) The primitive unit cell of ferroelectric GeTe, in which the purple arrow indicates the relative offsets between Ge and Te atoms along the *c*-axis. (b) The hexagonal supercell of GeTe, which consists of three Ge−Te pairs (i.e., Ge_1Te_1, Ge_2Te_2, and Ge_3Te_3) along the *c*-axis. (c) The hexagonal A-type antiferromagnet MnTe, in which spins of Mn ions (represented by arrows) align ferromagnetically in the hexagonal plane, with antiferromagnetic coupling along the *c*-axis. (d, e) The calculated band structures of GeTe and MnTe. The vertical dotted lines label the high-symmetry points, and the Fermi level is set at zero.

ideal rocksalt sites along the [111] direction (i.e., the *c*-axis in Figure 2a). Figure 2b displays the hexagonal unit cell of GeTe, in which three Ge−Te pairs (i.e., Ge_1Te_1, Ge_2Te_2, and Ge_3Te_3) are stacked in the order *ABCABC* along the ferroelectric polarization direction (i.e., the *c*-axis direction). GeTe is a ferroeletric semiconductor with a calculated band gap of about 0.65 eV, as seen in Figure 2d. The A-type antiferromagnet MnTe has a NiAs-type hexagonal phase,[43,44] as shown in Figure 2c. The two Mn−Te pairs (i.e., Mn_1Te_1 and Mn_2Te_2) are stacked in the order *ABAB* along the vertical direction. All of the quantitative data are calculated by the generalized gradient approximation (GGA)+*U* scheme[45] with U_{eff} = 0, unless mentioned otherwise. Although different U_{eff} values give rise to different calculated band gaps for MnTe, it does not change the conclusion of our investigation, which has been tested and summarized in the Supporting Information.

We construct supercells with the hexagonal MnTe and GeTe layers stacked along the *c*-axis. Four layers of GeTe and eight layers of MnTe are used. There is no need to further increase the thickness of the four-layer GeTe, as six and seven layers of GeTe have been tested and have shown similar results as four-layer GeTe. Considering the *ABC*-stacking of GeTe and the *AB*-stacking of MnTe, there are six different contacting

https://dx.doi.org/10.1021/acs.nanolett.0c02584
Nano Lett. XXXX, XXX, XXX−XXX

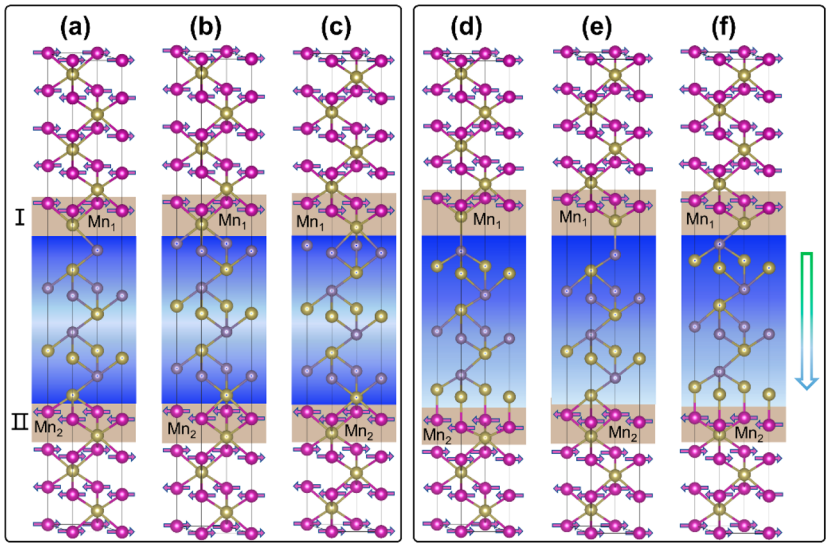

Figure 3. Atomic structures of the six GeTe/MnTe superlattices. Each superlattice consists of eight layers of MnTe and four layers of GeTe. (a−c) GeTe has no net polarization, and the relaxed lattice constant is about 4.15 Å. (d−f) GeTe is ferroelectric with the ferroelectric polarization pointing from dark blue to light gray, and the relaxed lattice constant is about 4.17 Å.

interfaces, as shown in Figure 3. The lateral lattice constants of the hexagonal GeTe and MnTe are 4.233 and 4.099 Å, respectively. The fully relaxed crystal structures are shown in Figure 3, in which the ferroelectric polarization of GeTe layers is indicated by the gradient from dark blue to light gray. The polarization pointing from light gray to dark blue is defined as the positive polarization.

The in-plane lattice constant a, the total energy per supercell E, the total magnetic moment per supercell M, and the induced magnetic moments of the interfacial Mn atoms are summarized in Table 1. The type-**f** structure with the ferroelectric phase has

Table 1. In-Plane Lattice Constant a, Total Energy per Supercell E, Total Net Magnetic Moment per Supercell M, and Magnetic Moments of the Interfacial $Mn_{1,2}$ Ions $m_{Mn1,2}$ of the Six Superlattices (a−f)

	paraelectric phase			ferroelectric phase		
	a	**b**	**c**	**d**	**e**	**f**
a (Å)	4.14	4.15	4.15	4.17	4.17	4.17
E (meV)	10	160	30	430	829	0
m_{Mn1} (μ_B)	4.041	4.059	4.044	3.913	3.919	3.988
m_{Mn2} (μ_B)	−4.048	−4.102	−4.056	−3.763	−3.990	−3.808
M (μ_B)	−0.008	−0.020	−0.008	0.095	−0.145	0.109

the lowest total energy, which is set as the reference energy (E = 0). For the superlattices illustrated in Figure 3a−c, they do not have net electric polarization, and the values of the magnetic moments of the interfacial Mn_1 and Mn_2 ions are nearly equal in amplitude and opposite in sign. However, for the superlattices illustrated in Figure 3d−f, GeTe layers have net electric polarization, and the differences between the absolute values of the magnetic moments of Mn_1 and Mn_2 ions are clear, resulting in net magnetic moments.

Figure 4 plots the density of states (DOS) of the six types of superlattices, in which red and blue curves represent the spin-up (α) and -down (β) channels, respectively. It is interesting that the superlattices in Figure 4a−c are nearly semiconductive, while those in Figure 4d−f are metallic and show more pronounced spin splitting around the Fermi level. Especially

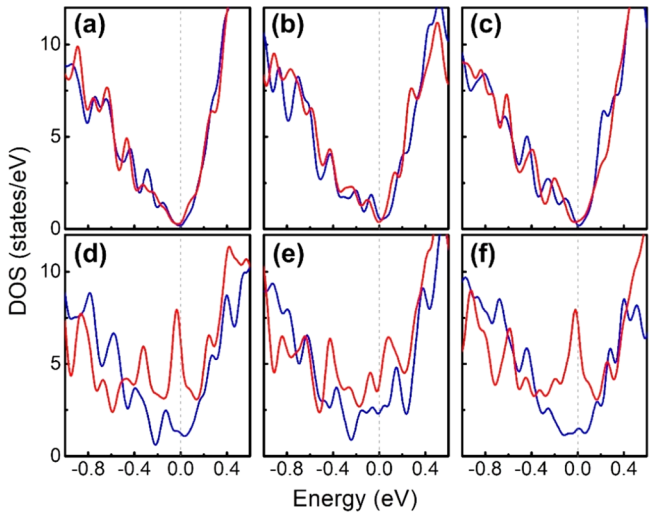

Figure 4. Spin-resolved total density of states (DOS) of the six superlattices. Parts a−c show the negligible spin polarization in the three superlattices consisting of paraelectric GeTe, as illustrated in Figure 3a−c. Parts d−f show the clearly lifted spin degeneracy in the three superlattices that consist of ferroelectric GeTe, as illustrated in Figure 3d−f. The red and blue lines represent spin-α and spin-β channels, respectively. The Fermi level is set at 0 eV.

for structure **f**, which has the lowest total energy, a nearly half-metallic character around the Fermi level is observed: the spin-α channel in red is dominant, while the spin-β in blue is suppressed. In Figure S2 of the Supporting Information, the DOS of the six superlattices for U_{eff} = 3 eV are shown, and similar to the case of U_{eff} = 0 eV, we obtain semiconductivity in the paraelectric superlattices and half-metallicity in the ferroelectric ones.

To investigate the effect of the ferroelectric polarization on the interfacial states of GeTe/MnTe, especially on the half-metallicity in structure **f**, we reverse the ferroelectric polarization in structure **f**. Parts a, c, and e of Figure 5 show the band structures for the paraelectric phase and negative and positive ferroelectric polarizations, respectively, in which the

https://dx.doi.org/10.1021/acs.nanolett.0c02584
Nano Lett. XXXX, XXX, XXX−XXX

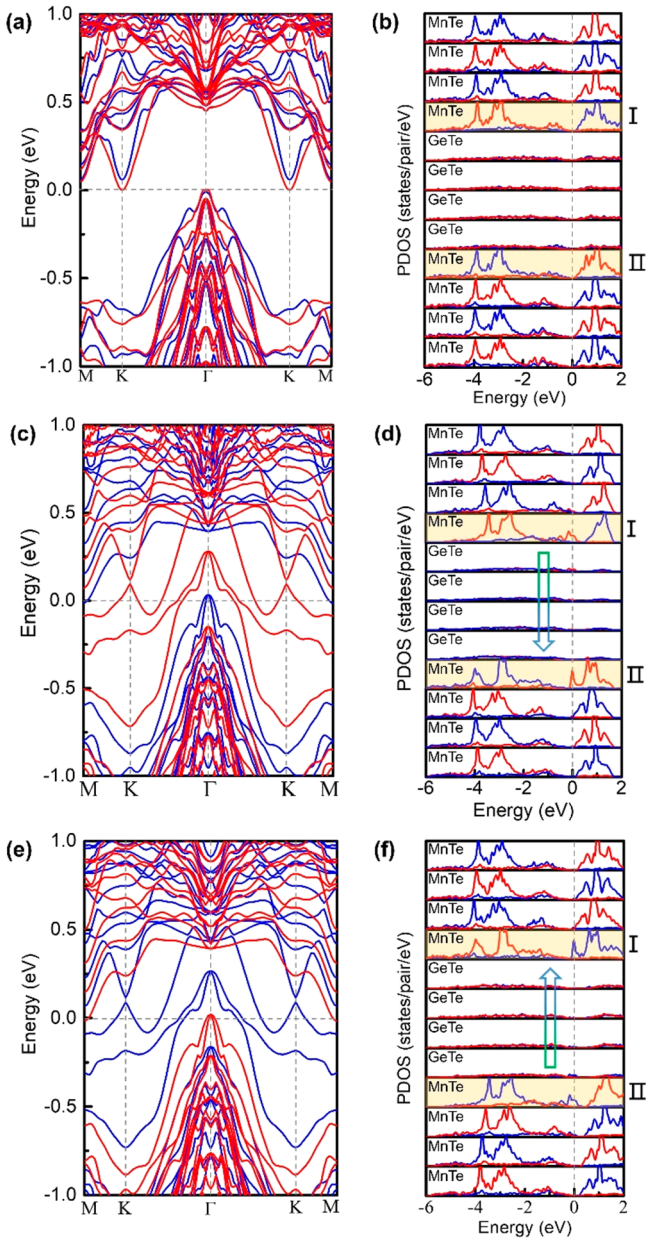

Figure 5. (a,c,e) The spin-resolved band structures and (b,d,f) the spin- and layer-resolved DOS of the superlattice of Figure 3f. In parts a and b, GeTe is paraelectric, in parts c and d, GeTe is negatively polarized, and in parts e and f, GeTe is positively polarized. The red and blue curves represent the spin-α and -β channels, respectively. The yellow shadows in parts b, d, and f indicate the interfacial MnTe layers.

red and blue curves indicate the spin-α and -β channels, respectively. These three band structures show that the superlattice remains semiconductive when GeTe is paraelectric but becomes metallic when GeTe is ferroelectric. Furthermore, the negative (positive) ferroelectric polarization results in the spin-α (spin-β) channels around the Fermi level (i.e., the reversal of the ferroelectric polarization can result in the reversal of the spin polarization). More specifically, in Figure 5d, when GeTe is negatively polarized, the states at the Fermi level completely arise from spin-α carriers (red curves); in Figure 5f, when GeTe is positively polarized, the states at the Fermi level completely arise from spin-β carriers (blue curves).

To understand the half-metallic interfacial states controlled by the ferroelectric polarization, we zoom in the details of the spin- and layer-resolved DOS in Figure 5d and f, in which the spin-α and -β channels are shown in red and blue, respectively. In Figure 5d, the ferroelectric polarization is pointing from up to down, leading to spin-α channels around the Fermi level, at both interfaces. The energy levels of the interface I are pushed to higher energy, so that the valence band of the MnTe layer at interface I crosses the Fermi level; concurrently, the energy levels of the interface II are pushed to lower energy, so that the conduction band of the MnTe layer at interface II crosses the Fermi level. These energy shifts result in spin-α holes at interface I and spin-α electrons at interface II, leading to spin-α half-metallicity in the superlattice. When the ferroelectric polarization is reversed (Figure 5f), the energy shifting behaviors are opposite, resulting in spin-β electrons at interface I and spin-β holes at interface II (i.e., spin-β half-metallicity in the superlattice). In Figure S3 of the Supporting Information, again we find similar results by using U_{eff} = 3 eV for Mn atoms.

Such a ferroelectric control of half-metallic states can be implemented to develop high-efficiency spin field-effect transistors (FETs), as illustrated in Figure S5 of the Supporting Information. The pure spin polarization can be created and annihilated by polarizing and depolarizing the ferroelectric and can be switched (between pure spin-up and pure spin-down) by flipping the ferroelectric polarization. Different from the conventional Datta−Das spin FET,[46] in which a precise control of spin precession based on Rashba spin orbit coupling[38,47] is demanded, the multiferroic spin FET proposed here is based on the spin polarization switching between spin-α and -β,[48,49] which is a lot easier to be realized in experiments. More remarkably, the spin polarization realized in our multiferroic FET is potentially approaching 100%, which would be otherwise an unlikely figure of merit in Datta−Das spin FET, fundamentally prohibited by spin-precession.

It is worthwhile to remark on the experimental feasibility of our proposed scheme. As is evident, the discussed mechanism and effect rely on the even-layer number of A-type antiferromagnet MnTe (i.e., a fully compensated antiferromagnet). A practical difference would be always unintentionally induced on the two neighboring interfaces of the superlattice in real experiments: one interface is formed by depositing MnTe onto GeTe, whereas the other, by depositing GeTe on MnTe. The difference of the two interfaces (e.g., the different local magnetic phase transition temperatures of the MnTe layers on the two interfaces) will cause one interface to enter into the magnetic phase first in field-cooling experiments, following the external magnetic field (see Figure S6 of the Supporting Information). The magnetization orientations of all of the remaining layers will be determined accordingly, which guarantees the MnTe layers at interface I and interface II always have opposite magnetizations (as depicted by Figure 1), which lays the foundation of the expected mechanism and outcomes.

In summary, half-metallicity, an intriguing state of 100% spin polarization arising from metallic electrons of one spin and insulating gap of the other spin, holds great potential for high-efficiency spintronic devices. By using first-principles calculations, we investigate the multiferroic semiconductor superlattice GeTe/MnTe, in which we obtain the half-metallicity and its ferroelectric control. We find that the half-metallicity can be created and annihilated by polarizing and depolarizing the ferroelectric and can be switched (between spin-up and

https://dx.doi.org/10.1021/acs.nanolett.0c02584
Nano Lett. XXXX, XXX, XXX−XXX

spin-down) by flipping the ferroelectric polarization. Based on this emergent mechanism, a new class of multiferroic spin field-effect transistors with electrically switchable spin current can be developed.

■ COMPUTATIONAL METHOD

First-principles calculations based on the density-functional theory (DFT) are performed to explore the electronic structures of the GeTe/MnTe superlattices, by using the projector augmented wave (PAW) method[50,51] implemented in the Vienna Ab initio Simulation Package (VASP).[52] In order to reduce the computational burden, we adopt the exchange correlation potential in the Perdew−Burke−Ernzerhof generalized gradient approximation (PBE-GGA) functional,[53] which can produce reasonable results for bulk GeTe and MnTe.[54] For the 3d orbital of the Mn atom, we use GGA+U with U_{eff} = 0 and 3 eV in the calculations. All of the results in the paper are based on U_{eff} = 0 eV, and the results corresponding to U_{eff} = 3 eV are presented in the Supporting Information. An energy cutoff of 500 eV for the plane wave expansion and an 11 × 11 × 2 k-point grid are used for the self-consistent calculations. The convergence of the total energy is checked by changing the number of sampling k-points and energy cutoff. The structures are fully relaxed until the Hellmann−Feynman forces on each atom are less than 1 meV/Å.

■ ASSOCIATED CONTENT

Supporting Information

The Supporting Information is available free of charge at https://pubs.acs.org/doi/10.1021/acs.nanolett.0c02584.

Additional data including the band structure of bulk MnTe (U_{eff} = 3 eV), the lattice constants, the magnetic moments, the DOS, and the band structures of the GeTe/MnTe superlattices (U_{eff} = 3 eV), the DOS of each ferromagnetic MnTe plane with U_{eff} = 0 and 3 eV, the schematic spin FET based on the GeTe/MnTe superlattice, and the remarks on the experimental feasibility of the proposed scheme (PDF)

■ AUTHOR INFORMATION

Corresponding Authors

Shi-Jing Gong − *Key Laboratory of Polar Materials and Devices (MOE), Department of Optoelectronics, East China Normal University, Shanghai 200241, China; Collaborative Innovation Center of Extreme Optics, Shanxi University, Taiyuan, Shanxi 030006, China; Shanghai Institute of Intelligent Electronics & Systems, Fudan University, Shanghai 200433, China;* Email: sjgong@ee.ecnu.edu.cn

Andrew M. Rappe − *Department of Chemistry, University of Pennsylvania, Philadelphia, Pennsylvania 19104, United States;* orcid.org/0000-0003-4620-6496; Email: rappe@sas.upenn.edu

Cheng Gong − *Department of Electrical and Computer Engineering and Quantum Technology Center, University of Maryland, College Park, Maryland 20742, United States;* orcid.org/0000-0001-7714-6380; Email: gongc@umd.edu

Authors

Er-Wei Du − *Key Laboratory of Polar Materials and Devices (MOE), Department of Optoelectronics, East China Normal University, Shanghai 200241, China*

Xiaodong Tang − *Key Laboratory of Polar Materials and Devices (MOE), Department of Optoelectronics, East China Normal University, Shanghai 200241, China*

Junhao Chu − *Department of Materials Science, Fudan University, Shanghai 200433, China*

Complete contact information is available at: https://pubs.acs.org/10.1021/acs.nanolett.0c02584

Author Contributions

#E.-W.D. and S.-J.G. contributed equally to this work.

Notes

The authors declare no competing financial interest.

■ ACKNOWLEDGMENTS

The work is supported by the National Key Research and Development Project 2019YFB2203403, the National Natural Science Foundation of China with Grant 61774059, National Natural Science Foundation of Shanghai with Grant 18ZR1412500, and ECNU Public Platform for Innovation (001). A.M.R. acknowledges support from the Department of Energy, Office of Science, Office of Basic Energy Sciences, under Grant No. DE-FG02-07ER46431.

■ REFERENCES

(1) Zhai, J.; Xing, Z.; Dong, S.; Li, J.; Viehland, D. Magnetoelectric Laminate Composites: An Overview. *J. Am. Ceram. Soc.* **2008**, *91*, 351−358.

(2) Nan, C.-W.; Bichurin, M. I.; Dong, S. X.; Viehland, D.; Srinivasan, G. Multiferroic magnetoelectric composites: Historical perspective, status, and future directions. *J. Appl. Phys.* **2008**, *103*, 031101.

(3) Spaldin, N. A.; Ramesh, R. Advances in magnetoelectric multiferroics. *Nat. Mater.* **2019**, *18*, 203.

(4) Spaldin, N. A.; Fiebig, M. The Renaissance of Magnetoelectric Multiferroics. *Science* **2005**, *309*, 391−392.

(5) Hu, J.-M.; Chen, L.-Q.; Nan, C.-W. Multiferroic Heterostructures Integrating Ferroelectric and Magnetic Materials. *Adv. Mater.* **2016**, *28*, 15−39.

(6) Fiebig, M.; Lottermoser, T.; Meier, D.; Trassin, M. The evolution of multiferroics. *Nat. Rev. Mater.* **2016**, *1*, 16046.

(7) Ederer, C.; Spaldin, N. A. Weak ferromagnetism and magnetoelectric coupling in bismuth ferrite. *Phys. Rev. B: Condens. Matter Mater. Phys.* **2005**, *71*, 060401.

(8) Van Aken, B. B.; Palstra, T. T. M.; Filippetti, A.; Spaldin, N. A. The origin of ferroelectricity in magnetoelectric $YMnO_3$. *Nat. Mater.* **2004**, *3*, 164.

(9) Lottermoser, T.; Lonkai, T.; Amann, U.; Hohlwein, D.; Ihringer, J.; Fiebig, M. Magnetic phase control by an electric field. *Nature* **2004**, *430*, 541.

(10) Kimura, T.; Kawamoto, S.; Yamada, I.; Azuma, M.; Takano, M.; Tokura, Y. Magnetocapacitance effect in multiferroic $BiMnO_3$. *Phys. Rev. B: Condens. Matter Mater. Phys.* **2003**, *67*, 180401.

(11) Kimura, T.; Goto, T.; Shintani, H.; Ishizaka, K.; Arima, T.; Tokura, Y. Magnetic control of ferroelectric polarization. *Nature* **2003**, *426*, 55.

(12) Kenzelmann, M.; Harris, A. B.; Jonas, S.; Broholm, C.; Schefer, J.; Kim, S. B.; Zhang, C. L.; Cheong, S.-W.; Vajk, O. P.; Lynn, J. W. Magnetic Inversion Symmetry Breaking and Ferroelectricity in $TbMnO_3$. *Phys. Rev. Lett.* **2005**, *95*, 087206.

(13) Cheong, S.-W.; Mostovoy, M. Multiferroics: a magnetic twist for ferroelectricity. *Nat. Mater.* **2007**, *6*, 13.

(14) Catalan, G.; Scott, J. F. Physics and Applications of Bismuth Ferrite. *Adv. Mater.* **2009**, *21*, 2463−2485.

(15) Solovyev, I. V.; Pchelkina, Z. V. Magnetic-field control of the electric polarization in $BiMnO_3$. *Phys. Rev. B: Condens. Matter Mater. Phys.* **2010**, *82*, 094425.

(16) Cherifi, R. O.; Ivanovskaya, V.; Phillips, L. C.; Zobelli, A.; Infante, I. C.; Jacquet, E.; Garcia, V.; Fusil, S.; Briddon, P. R.; Guiblin, N.; et al. Electric-field control of magnetic order above room temperature. *Nat. Mater.* **2014**, *13*, 345.
(17) Wu, S. M.; Cybart, S. A.; Yi, D.; Parker, J. M.; Ramesh, R.; Dynes, R. C. Full Electric Control of Exchange Bias. *Phys. Rev. Lett.* **2013**, *110*, 067202.
(18) Zhang, S.; Zhao, Y. G.; Li, P. S.; Yang, J. J.; Rizwan, S.; Zhang, J. X.; Seidel, J.; Qu, T. L.; Yang, Y. J.; Luo, Z. L.; et al. Electric-Field Control of Nonvolatile Magnetization in $Co_{40}Fe_{40}B_{20}$/Pb-$(Mg_{1/3}Nb_{2/3})_{0.7}Ti_{0.3}O_3$ Structure at Room Temperature. *Phys. Rev. Lett.* **2012**, *108*, 137203.
(19) Eerenstein, W.; Wiora, M.; Prieto, J. L.; Scott, J. F.; Mathur, N. D. Giant sharp and persistent converse magnetoelectric effects in multiferroic epitaxial heterostructures. *Nat. Mater.* **2007**, *6*, 348.
(20) Zheng, H.; Wang, J.; Lofland, S. E.; Ma, Z.; Mohaddes-Ardabili, L.; Zhao, T.; Salamanca-Riba, L.; Shinde, S. R.; Ogale, S. B.; Bai, F.; et al. Multiferroic $BaTiO_3$-$CoFe_2O_4$ Nanostructures. *Science* **2004**, *303*, 661−663.
(21) Mundy, J. A.; Brooks, C. M.; Holtz, M. E.; Moyer, J. A.; Das, H.; Rébola, A. F.; Heron, J. T.; Clarkson, J. D.; Disseler, S. M.; Liu, Z. Q.; et al. Atomically engineered ferroic layers yield a room-temperature magnetoelectric multiferroic. *Nature* **2016**, *537*, 523.
(22) Heron, J. T.; Trassin, M.; Ashraf, K.; Gajek, M.; He, Q.; Yang, S. Y.; Nikonov, D. E.; Chu, Y.-H.; Salahuddin, S.; Ramesh, R. Electric-Field-Induced Magnetization Reversal in a Ferromagnet-Multiferroic Heterostructure. *Phys. Rev. Lett.* **2011**, *107*, 217202.
(23) Wu, S. M.; Cybart, S. A.; Yu, P.; Rossell, M. D.; Zhang, J. X.; Ramesh, R.; Dynes, R. C. Reversible electric control of exchange bias in a multiferroic field-effect device. *Nat. Mater.* **2010**, *9*, 756.
(24) Vaz, C. A. F.; Hoffman, J.; Ahn, C. H.; Ramesh, R. Magnetoelectric Coupling Effects in Multiferroic Complex Oxide Composite Structures. *Adv. Mater.* **2010**, *22*, 2900−2918.
(25) Chu, Y.-H.; Martin, L. W.; Holcomb, M. B.; Gajek, M.; Han, S.-J.; He, Q.; Balke, N.; Yang, C.-H.; Lee, D.; Hu, W.; et al. Electric-field control of local ferromagnetism using a magnetoelectric multiferroic. *Nat. Mater.* **2008**, *7*, 478.
(26) Gong, C.; Kim, E. M.; Wang, Y.; Lee, G.; Zhang, X. Multiferroicity in atomic van der Waals heterostructures. *Nat. Commun.* **2019**, *10*, 2657.
(27) Meng, Y.-H.; Bai, W.; Gao, H.; Gong, S.-J.; Wang, J.-Q.; Duan, C.-G.; Chu, J.-H. Ferroelectric control of Rashba spin orbit coupling at the GeTe (111)/InP (111) interface. *Nanoscale* **2017**, *9*, 17957−17962.
(28) Liebmann, M.; Rinaldi, C.; Di Sante, D.; Kellner, J.; Pauly, C.; Wang, R. N.; Boschker, J. E.; Giussani, A.; Bertoli, S.; Cantoni, M.; et al. Giant Rashba-Type Spin Splitting in Ferroelectric GeTe(111). *Adv. Mater.* **2016**, *28*, 560−565.
(29) Di Sante, D.; Barone, P.; Bertacco, R.; Picozzi, S. Electric Control of the Giant Rashba Effect in Bulk GeTe. *Adv. Mater.* **2013**, *25*, 509−513.
(30) Gong, S.-J.; Zheng, F.; Rappe, A. M. Phonon Influence on Bulk Photovoltaic Effect in the Ferroelectric Semiconductor GeTe. *Phys. Rev. Lett.* **2018**, *121*, 017402.
(31) He, Q. L.; Yin, G.; Grutter, A. J.; Pan, L.; Che, X. Y.; Yu, G. Q.; Gilbert, D. A.; Disseler, S. M.; Liu, Y. Z.; Shafer, P.; et al. Exchange-biasing topological charges by antiferromagnetism. *Nat. Commun.* **2018**, *9*, 2767.
(32) Kriegner, D.; Výborný, K.; Olejník, K.; Reichlová, H.; Novák, V.; Marti, X.; Gazquez, J.; Saidl, V.; Němec, P.; Volobuev, V. V.; et al. Multiple-stable anisotropic magnetoresistance memory in antiferromagnetic MnTe. *Nat. Commun.* **2016**, *7*, 11623.
(33) Kriegner, D.; Reichlova, H.; Grenzer, J.; Schmidt, W.; Ressouche, E.; Godinho, J.; Wagner, T.; Martin, S. Y.; Shick, A. B.; Volobuev, V. V.; et al. Magnetic anisotropy in antiferromagnetic hexagonal MnTe. *Phys. Rev. B: Condens. Matter Mater. Phys.* **2017**, *96*, 214418.
(34) Yin, G.; Yu, J.-X.; Liu, Y. Z.; Lake, R. K.; Zang, J. D.; Wang, K. L. Planar Hall Effect in Antiferromagnetic MnTe Thin Films. *Phys. Rev. Lett.* **2019**, *122*, 106602.
(35) Chen, W. Q.; Teo, K. L.; Lim, S. T.; Jalil, M. B. A.; Liew, T.; Chong, T. C. Magnetic and transport behaviors in $Ge_{1-x}Mn_xTe$ with high Mn composition. *Appl. Phys. Lett.* **2007**, *90*, 142514.
(36) Fukuma, Y.; Asada, H.; Miyawaki, S.; Koyanagi, T.; Senba, S.; Goto, K.; Sato, H. Carrier-induced ferromagnetism in $Ge_{0.92}Mn_{0.08}Te$ epilayers with a Curie temperature up to 190 K. *Appl. Phys. Lett.* **2008**, *93*, 252502.
(37) Lechner, R. T.; Springholz, G.; Hassan, M.; Groiss, H.; Kirchschlager, R.; Stangl, J.; Hrauda, N.; Bauer, G. Phase separation and exchange biasing in the ferromagnetic IV-VI semiconductor $Ge_{1-x}Mn_xTe$. *Appl. Phys. Lett.* **2010**, *97*, 023101.
(38) Krempaský, J.; Muff, S.; Bisti, F.; Fanciulli, M.; Volfová, H.; Weber, A. P.; Pilet, N.; Warnicke, P.; Ebert, H.; Braun, J.; et al. Entanglement and manipulation of the magnetic and spin-orbit order in multiferroic Rashba semiconductors. *Nat. Commun.* **2016**, *7*, 13071.
(39) Kriegner, D.; Furthmüller, J.; Kirchschlager, R.; Endres, J.; Horak, L.; Cejpek, P.; Reichlova, H.; Marti, X.; Primetzhofer, D.; Ney, A.; et al. Ferroelectric phase transitions in multiferroic $Ge_{1-x}Mn_xTe$ driven by local lattice distortions. *Phys. Rev. B: Condens. Matter Mater. Phys.* **2016**, *94*, 054112.
(40) Przybylińska, H.; Springholz, G.; Lechner, R. T.; Hassan, M.; Wegscheider, M.; Jantsch, W.; Bauer, G. Magnetic-Field-Induced Ferroelectric Polarization Reversal in the Multiferroic $Ge_{1-x}Mn_xTe$ Semiconductor. *Phys. Rev. Lett.* **2014**, *112*, 047202.
(41) Kriener, M.; Nakajima, T.; Kaneko, Y.; Kikkawa, A.; Hashizume, D.; Kato, K.; Takata, M.; Arima, T.; Tokura, Y.; Taguchi, Y. Enhanced ferromagnetic transition temperature induced by a microscopic structural rearrangement in the diluted magnetic semiconductor $Ge_{1-x}Mn_xTe$. *Phys. Rev. B: Condens. Matter Mater. Phys.* **2017**, *95*, 224418.
(42) Kriener, M.; Nakajima, T.; Kaneko, Y.; Kikkawa, A.; Yu, X. Z.; Endo, N.; Kato, K.; Takata, M.; Arima, T.; Tokura, Y.; et al. Heat-Treatment-Induced Switching of Magnetic States in the Doped Polar Semiconductor $Ge_{1-x}Mn_xTe$. *Sci. Rep.* **2016**, *6*, 25748.
(43) Szuszkiewicz, W.; Dynowska, E.; Witkowska, B.; Hennion, B. Spin-wave measurements on hexagonal MnTe of NiAs-type structure by inelastic neutron scattering. *Phys. Rev. B: Condens. Matter Mater. Phys.* **2006**, *73*, 104403.
(44) Mu, S.; Hermann, R. P.; Gorsse, S.; Zhao, H. Z.; Manley, M. E.; Fishman, R. S.; Lindsay, L. Phonons, magnons, and lattice thermal transport in antiferromagnetic semiconductor MnTe. *Phys. Rev. Mater.* **2019**, *3*, 025403.
(45) Anisimov, V. I.; Zaanen, J.; Andersen, O. K. Band theory and Mott insulators: Hubbard *U* instead of Stoner. *Phys. Rev. B: Condens. Matter Mater. Phys.* **1991**, *44*, 943.
(46) Datta, S.; Das, B. Electronic analog of the electro-optic modulator. *Appl. Phys. Lett.* **1990**, *56*, 665−667.
(47) Manchon, A.; Koo, H. C.; Nitta, J.; Frolov, S. M.; Duine, R. A. New perspectives for Rashba spin-orbit coupling. *Nat. Mater.* **2015**, *14*, 871.
(48) Gong, C.; Zhang, X. Two-dimensional magnetic crystals and emergent heterostructure devices. *Science* **2019**, *363*, No. eaav4450.
(49) Gong, S.-J.; Gong, C.; Sun, Y.-Y.; Tong, W.-Y.; Duan, C.-G.; Chu, J.-H.; Zhang, X. Electrically induced 2D half-metallic antiferromagnets and spin field effect transistors. *Proc. Natl. Acad. Sci. U. S. A.* **2018**, *115*, 8511−8516.
(50) Blöchl, P. E. Projector augmented-wave method. *Phys. Rev. B: Condens. Matter Mater. Phys.* **1994**, *50*, 17953.
(51) Kresse, G.; Joubert, D. From ultrasoft pseudopotentials to the projector augmented-wave method. *Phys. Rev. B: Condens. Matter Mater. Phys.* **1999**, *59*, 1758.
(52) Kresse, G.; Furthmüller, J. Efficiency of ab-initio total energy calculations for metals and semiconductors using a plane-wave basis set. *Comput. Mater. Sci.* **1996**, *6*, 15−50.
(53) Perdew, J. P.; Burke, K.; Ernzerhof, M. Generalized Gradient Approximation Made Simple. *Phys. Rev. Lett.* **1996**, *77*, 3865.

https://dx.doi.org/10.1021/acs.nanolett.0c02584
Nano Lett. XXXX, XXX, XXX−XXX

(54) Krukau, A. V.; Vydrov, O. A.; Izmaylov, A. F.; Scuseria, G. E. Influence of the exchange screening parameter on the performance of screened hybrid functionals. *J. Chem. Phys.* **2006**, *125*, 224106.

https://dx.doi.org/10.1021/acs.nanolett.0c02584
Nano Lett. XXXX, XXX, XXX−XXX